Materials Performance and Characterization

doi:10.1520/MPC20170115 / Vol. 7 / No. 2 / 2018 / available online at www.astm.org

Kien Nguyen,[1] Reza Nasouri,[2] Caroline R. Bennett,[3] Adolfo Matamoros,[2] Jian Li,[1] and Arturo H. Montoya[2]

Thermomechanical Modeling of Welding and Galvanizing a Steel Beam Connection Detail to Examine Susceptibility to Cracking

Reference

Nguyen, K., Nasouri, R., Bennett, C. R., Matamoros, A., Li, J., and Montoya, A. H., "Thermomechanical Modeling of Welding and Galvanizing a Steel Beam Connection Detail to Examine Susceptibility to Cracking," *Materials Performance and Characterization*, Vol. 7, No. 2, 2018, pp. 165–190, https://doi.org/10.1520/MPC20170115. ISSN 2379-1365

ABSTRACT

Hot-dip galvanizing is the process of submerging steel elements into molten zinc to form a metallurgically bonded zinc coating that serves as corrosion protection for the steel substrate. Used with great success on an industrial scale for many decades, hot-dip galvanizing is a ubiquitous process. On occasion, cracks in steel members develop during galvanizing. While such cracking remains a poorly understood phenomenon, previous research has attributed the formation of cracks to the combined effects of residual strains introduced by welding and temperature-induced deformations caused by the hot-dip galvanizing process. This article presents thermomechanical analyses of a structural steel beam with a welded double-angle connection detail where cracking occurred during hot-dip galvanizing. Three-dimensional finite element models of the beam and connection detail were analyzed using the finite element analysis software Abaqus (Dassault Systèmes, Vélizy-Villacoublay, France). The welding process was simulated using the Abaqus Welding Interface, maintaining the welding sequence of the connection. After welding, the entire beam was subjected to a temperature field that was specified through a user subroutine in Abaqus, simulating the hot-dip galvanizing process. The temperature field had a bath temperature of 450°C and a thermal cycle that included dipping, dwell time, and removal from the bath. Material properties used in the simulation were nonlinear

Manuscript received July 21, 2017; accepted for publication November 30, 2017; published online July 10, 2018.

[1] Department of Civil, Environmental and Architectural Engineering, University of Kansas, 1530 W. 15th St., 2150 Learned Hall, Lawrence, KS 66045, USA, https://orcid.org/0000-0003-0745-9984 (K.N.)

[2] Department of Civil and Environmental Engineering, University of Texas at San Antonio, 1 UTSA Cir., San Antonio, TX 78249, USA

[3] Department of Civil, Environmental and Architectural Engineering, University of Kansas, 1530 W. 15th St., 2150 Learned Hall, Lawrence, KS 66045, USA (Corresponding author), e-mail: crb@ku.edu, https://orcid.org/0000-0002-2713-0011

Copyright by ASTM Int'l (all rights reserved); Wed Dec 4 09:43:32 EST 2019
Copyright © 2018 by ASTM International, 100 Barr Harbor Drive, PO Box C700, West Conshohocken, PA 19428-2959

Downloaded/printed by
Kansas University (Kansas University) pursuant to License Agreement. No further reproductions authorized.

and temperature dependent. The parameters of the study were the welding sequences, heat input during welding, and the depth of the double-angle connection. It was observed that strain demands due to welding and hot-dip galvanizing were high magnitude at the cracked location in the beam. The relative significance of strain demands due to welding and of hot-dip galvanizing on the propensity for the beam to develop cracks are discussed.

Keywords

welding residual stress, thermal stress, cracking, hot-dip galvanizing, steel building structures, finite element analysis

Introduction

Corrosion damage of steel structures has been estimated to be as high as 3.0 % of the gross domestic product of many countries, including the United States, making it a matter of significant concern [1,2]. Hot-dip galvanizing, a common industrial process used to prevent corrosion, has been used with success on a large scale for many decades. In this process, steel elements are cleaned through a surface preparation process and then submerged into molten zinc to form a metallurgically bonded zinc coating that serves as corrosion protection for the steel substrate.

On occasion, incidents of cracking in steel structures have been documented during the galvanizing process. Such cracks require costly repairs and raise safety concerns when structures with undetected flaws are placed in service. While cracking associated with galvanizing remains a poorly understood phenomenon, previous research has concluded that the combined effects of residual strains introduced by fabrication (e.g., rolling and straightening, welding, bending, cutting, punching) and strain demands caused by the hot-dip galvanizing process [3,4] are important contributing factors to the formation of cracks.

A W8×18 steel beam (metric equivalent W200×135×26.6) with a welded double clip angle connection (L3×3×3/8, metric equivalent L75×75×9.5) was found to have sustained cracking during hot-dip galvanizing (Fig. 1). The crack opened at a distance of 4 mm from the weld toe, at the beam end, and paralleled the weld line for 75 mm, although the location of crack initiation was not apparent. This type of connection detail is common in building

FIG. 1

Beam detail with crack after hot-dip galvanizing.

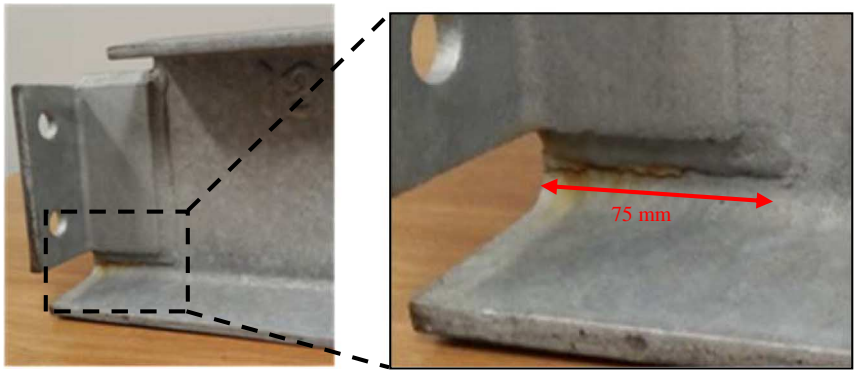

Copyright by ASTM Int'l (all rights reserved); Wed Dec 4 09:43:32 EST 2019
Downloaded/printed by
Kansas University (Kansas University) pursuant to License Agreement. No further reproductions authorized.

structures, so this failure raised concern among designers, fabricators, and galvanizers and highlighted the need to investigate the problem.

Since physical tests are expensive and highly challenging, especially in hot-dip galvanizing conditions where testing devices are submerged in a high-temperature (450°C) liquid zinc environment, computational simulations offer a useful tool with which to study the cracking phenomenon. Even so, thermomechanical analyses that simulate both the welding and galvanizing processes are technically challenging and require large computer platforms, which explains the sparse literature pertaining to such simulations. Toi, Kobashi, and Iezawa [5] analyzed the behavior of welded bridge girders during hot-dip galvanizing but did not account for the effect of welding. Later, Toi and Lee [6] incorporated measured welding residual stress into the finite element model as an initial condition. An important study was performed by Kleineck [7], who modeled steel high mast illumination poles to investigate galvanizing-induced cracks at the weld toe of the connection between the base plate and pole shaft. However, this study did not account for the effects of the welding process. Rudd et al. [8] numerically investigated the strain history of several steel details during the galvanizing process, but did not include the effect of strains induced by the welding process.

The objectives of this study were to (1) study the behavior of a welded beam connection during the galvanizing process, identifying areas with the highest susceptibility to cracking, and (2) to study the effect of the propensity to crack on three parameters that are commonly varied in design and fabrication practice: welding sequence, welding heat input, and the depth of the double-angle connection. Three-dimensional finite element models of the W8×18 beam were analyzed using thermomechanical analyses with load steps simulating the sequential effects of welding and hot-dip galvanizing. The analyses included material and geometric nonlinearities, and the properties of the steel were temperature dependent.

Finite Element Model

GENERAL DESCRIPTION

A sequentially coupled thermal-stress analysis using Abaqus (Dassault Systèmes, Vélizy-Villacoublay, France) was developed to capture the cumulative effect of both welding and galvanizing processes on the beam detail shown in **Fig. 1**. The loading sequence began with a nonlinear heat transfer analysis that simulated the welding sequence and the galvanizing process. The calculated temperature fields were then imposed on the beam section to calculate stress and strain fields. This sequential modeling approach has been used widely to simulate welding processes in the literature, including studies performed by Deng and Murakawa [9], Perić et al. [10], and Keinänen [11]. This approach provides the opportunity to study the influence of welding parameters (and the ensuing residual stresses and strains) on stress and strain responses during and after galvanizing.

Thermomechanical properties of S355JR steel (equivalent to ASTM A572-50, *Standard Specification for High-Strength Low-Alloy Columbium-Vanadium Structural Steel*) were sourced from Perić et al. [10]. Temperature-dependent thermal and mechanical properties (**Fig. 2**) were the same for the weld and base metal; the phase transformation of welding was neglected in this analysis because of its insignificant effect [9]. In addition to being temperature dependent, the material model for steel was elastic-plastic.

The beam section and connection detail were representative of the actual sample that cracked during galvanizing. It included an I-beam (W8×18, metric equivalent

Copyright by ASTM Int'l (all rights reserved); Wed Dec 4 09:43:32 EST 2019
Downloaded/printed by
Kansas University (Kansas University) pursuant to License Agreement. No further reproductions authorized.

FIG. 2

Temperature-dependent material properties: (a) thermal and (b) elastic-plastic mechanical, adapted from Perić et al. [10].

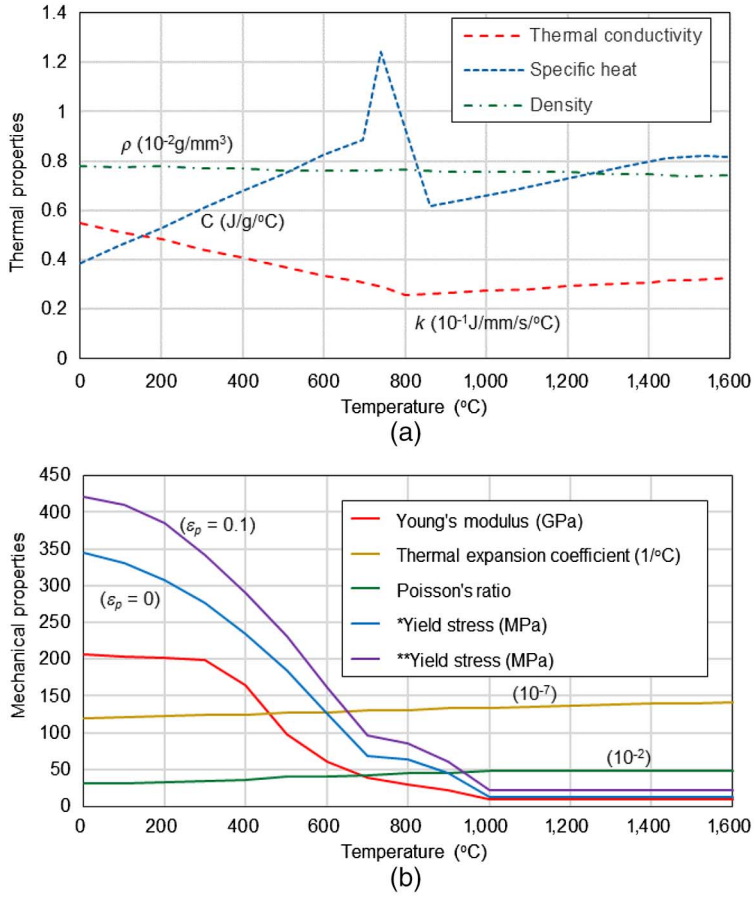

W200×135×26.6) and two clip angles (L3×3×3/8, metric equivalent L75×75×9.5), as presented in Fig. 3. The double angles were welded onto the beam section using techniques that are described in more detail in the next section. Although weld size varied from location to location in the physical beam, a 6-mm fillet weld was modeled on both sides of the beam, and a weld size of 5.0 by 5.8 mm was assigned to the vertical weld at the beam end between the two clip angles. A beam cope was modeled at the top flange with a depth of 30 mm, a length of 76 mm, and a radius of 10 mm. Bolt holes on the outstanding legs of the double angles were included in the model and had a diameter of 22 mm. All of these dimensions were based on measurements of the beam. Fig. 3 also shows the boundary conditions, which were selected to minimize their effects on the stress and strain fields in the area surrounding the connection detail.

The mesh configuration was designed based on the results from a mesh sensitivity study. The beam web, with a thickness of 5.8 mm, had four elements through its thickness, as did the two beam flanges. The clip angles were three elements thick. The region surrounding the weld lines was meshed using edge seeding with a size of 1.5 mm in the longitudinal direction to accurately represent the temperature and strain gradients. A typical element size used in the mesh surrounding the observed crack area was 1.10 by 1.45 by 1.50 mm. The entire model included approximately 193,000 elements and 217,000 nodes.

Copyright by ASTM Int'l (all rights reserved); Wed Dec 4 09:43:32 EST 2019
Downloaded/printed by
Kansas University (Kansas University) pursuant to License Agreement. No further reproductions authorized.

FIG. 3 Dimensions, boundary conditions, and meshing of the control model.

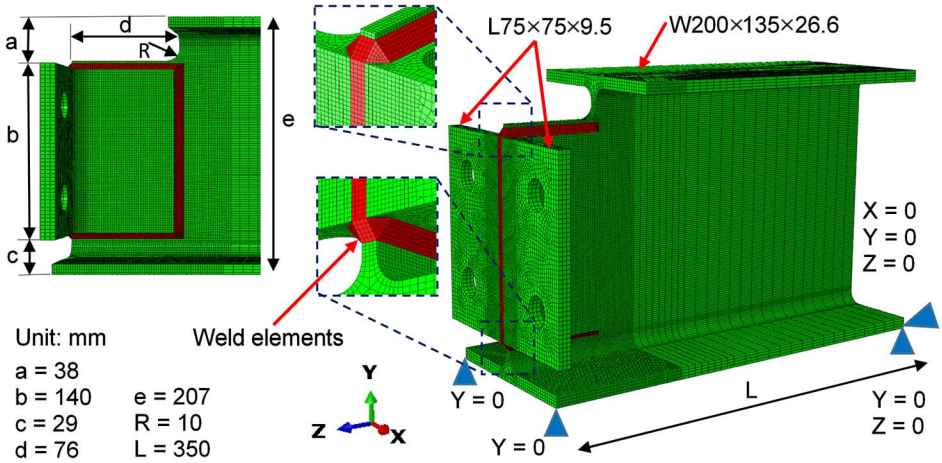

For the thermal analysis, eight-node linear heat transfer brick elements were used; for the stress analysis, eight-node linear brick elements were used.

Calculated total strains were decomposed into three components: elastic, plastic, and thermal strain. Elastic strain was calculated based on the isotropic Hooke's law with temperature-dependent values for Young's modulus and Poisson's ratio (Fig. 2). Thermal strain was calculated using the coefficient of thermal expansion, which was also temperature dependent (Fig. 2). Plastic strain was independent of loading rate but dependent on temperature (Fig. 2).

Linear kinematic hardening was utilized to capture material behavior during welding [12]. The selection of a hardening model is an important choice for this type of analysis, and it has been discussed extensively in the literature [13–19]. Although the use of a combined model of kinematic and isotropic hardening would be preferable, obtaining the experimental data to calibrate it is extremely difficult because of the effects that temperature has on the mechanical properties of the steel. Nonlinear material behavior was included in the model using incremental plasticity with the von Mises yield criterion and the associated plastic flow rule [20].

WELD SIMULATION METHODOLOGY

The welding simulation was performed using the Abaqus Welding Interface (AWI) plug-in, a utility developed by SIMULIA [21]. The AWI utility generates analysis steps for the heat transfer and static stress analyses, bypassing the need for the user to manually define hundreds of steps in which a weld is placed in small segments over the area to be welded. Welding parameters are input by the user in the AWI utility, specifying welding speed, welding sequence, weld and base metal material, and heat transfer properties. In the heat transfer analysis, the weld is simulated via a prescribed temperature applied at the boundary between the current weld pass and the base metal. The applied temperature is then ramped (at a user-defined rate) and held over a period of time, after which a user-defined segment of weld elements is deposited into the weld pool. Each length of weld segment includes the full weld cross-section. An illustration of the prescribed temperature approach implemented using the AWI utility is presented in Fig. 4. The output temperature

Copyright by ASTM Int'l (all rights reserved); Wed Dec 4 09:43:32 EST 2019
Downloaded/printed by
Kansas University (Kansas University) pursuant to License Agreement. No further reproductions authorized.

FIG. 4

The prescribed temperature approach for nodes associated with a weld, modified from Lindgren [17].

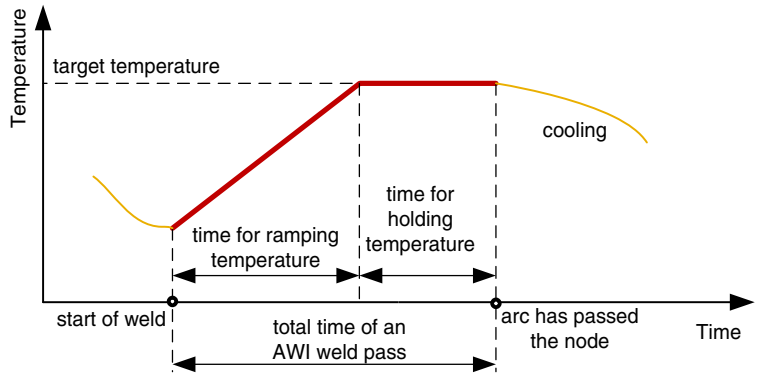

fields of the heat transfer analysis are then applied as a predefined condition in the stress (mechanical) analysis. During this analysis, all weld elements are already present. However, the yet-to-be-deposited weld elements are assigned a melting temperature (1,450°C), which leads to very soft mechanical properties for the weld elements. This allows the yet-to-be-deposited weld elements to deform with weld zone deformation, thereby not affecting the overall response. The deposition of weld metal during the stress analysis is handled in the AWI utility using the "model change" technique in Abaqus to remove and reintroduce the corresponding weld elements with a free strain state [22]. A full description of the analysis methodology and numerical steps used in the AWI modeling routine can be found in the AWI Users' Manual [21].

Fig. 5 shows the welding sequence used in the control model of this study. The welding speed was $v = 400$ mm/min. The heat convective coefficient in air was $h_{air} = 10$ W/m^2/K [10,23,24]. The effective emissivity was $\varepsilon = 0.9$, and the Stefan-Boltzmann constant was $\sigma = 5.67\text{E-}08$. Room temperature was specified to be 20°C. After the welding process was completed, the beam was allowed to cool for 3,600 s before the galvanizing sequence was initiated in the model.

A sensitivity study of the AWI model input parameters was presented by Nguyen et al. [25]. The goal of that study was to determine sets of AWI interface input parameters that would produce results in good agreement with experimental measurements. Based on the sensitivity study by Nguyen et al. [25], a prescribed temperature of 1,500°C (slightly higher than the melting temperature of steel of 1,450°C) and a weld segment length of 10 mm were chosen. The third parameter, the ramping option in the AWI utility, was used to change the welding heat input parameter. The ramping option allows the user to adjust the speed at which the welding target temperature is achieved, thereby affecting weld heat input. Note that this technique is helpful for adjusting heat input for a given weld size, but heat input can also be influenced by the weld dimensions. The use of these parameter-generated temperature profiles that were close to the experimental measurements were obtained by Perić et al. [10].

GALVANIZING SIMULATION METHODOLOGY

The thermal and mechanical analyses for the hot-dip galvanizing process were embedded after the welding simulation was completed. The Abaqus user subroutine, FILM, was developed to simulate the external temperature field acting on the beam as it was being

Copyright by ASTM Int'l (all rights reserved); Wed Dec 4 09:43:32 EST 2019
Downloaded/printed by
Kansas University (Kansas University) pursuant to License Agreement. No further reproductions authorized.

FIG. 5 Timeline of the welding simulation (welding sequence 1 is shown).

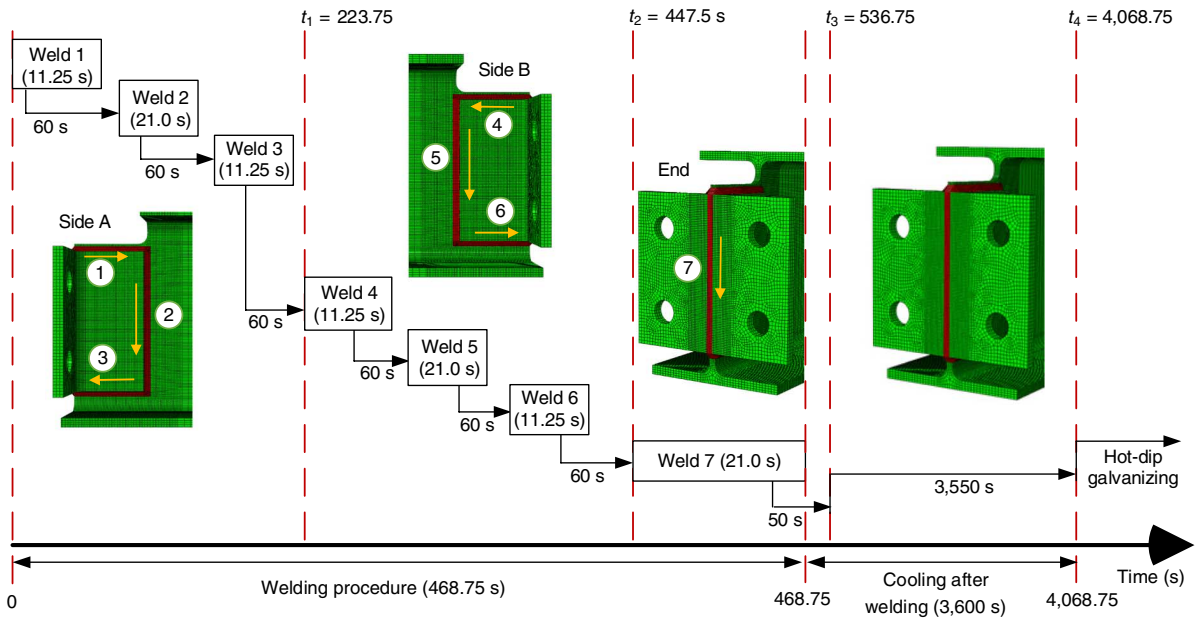

dipped, held, and extracted from a galvanizing kettle, as illustrated in Fig. 6. The FILM subroutine was responsible for creating a reference plane, which moved across the beam model based on the dipping velocity. The portions of the beam detail below the reference plane were assigned parameters representing contact with liquid zinc; the portions above the reference plane were assigned parameters representing contact with air. While steel parts were in contact with liquid zinc in the galvanizing bath, convection between the molten zinc and the structural component was considered to be the primary mode of heat transfer, while radiation and conduction were assumed negligible. The heat convective coefficient used when the beam was in contact with liquid zinc was $h_{zinc} = 1{,}350$ W/m^2/K and was $h_{air} = 10$ W/m^2/K when the beam was in contact with air; both of these coefficients were derived experimentally by Cresdee et al. [26]. The air temperature was set to 20°C, and the liquid zinc temperature was set to 450°C. Dipping and removing speeds of 300 mm/min were chosen based on common practice. The beam section was modeled as being dipped with an angle of 0°, meaning the connection detail was dipped horizontally. The beam was held fully submerged in the bath for 320 s (referred to as the dwell time). The total time for the galvanizing process, including dipping, dwelling, and extraction, was 400 s. After extraction, the beam model was allowed to cool in-air for 3,600 s.

To examine the effect of welding and hot-dip galvanizing on the beam detail, eleven key points of time were selected across the sequential process and are denoted as t_1–t_{11}, as shown in Figs. 5 and 6. The physical significance of each of those points is described in Table 1.

PARAMETRIC STUDY

The effects of three parameters on the stress and strain fields in the beam-end connection were evaluated: welding sequence, welding heat input, and geometry of the connection.

Copyright by ASTM Int'l (all rights reserved); Wed Dec 4 09:43:32 EST 2019
Downloaded/printed by
Kansas University (Kansas University) pursuant to License Agreement. No further reproductions authorized.

FIG. 6 Timeline of hot-dip galvanizing simulation.

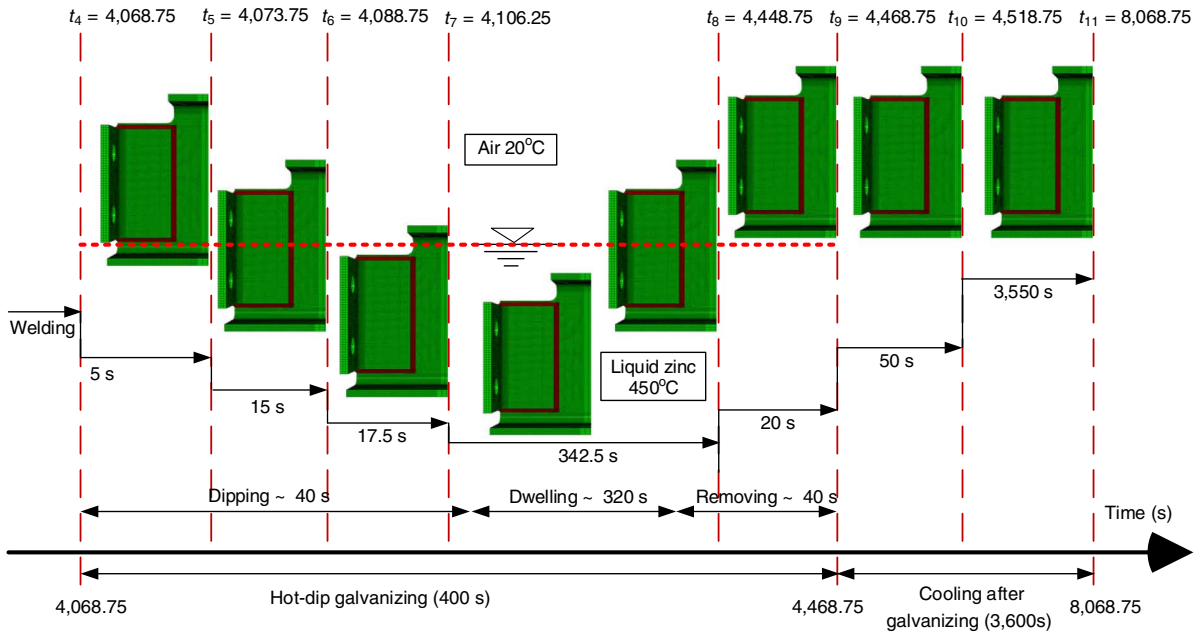

TABLE 1
Explanation of time points shown in **Fig. 5** and **Fig. 6**.

Time	Significance
t_1	60 s after finishing Welds 1, 2, and 3 at Side A
t_2	60 s after finishing Welds 4, 5, and 6 on Side B
t_3	50 s after finishing Weld 7 at the beam end
t_4	3,600 s after the postweld cooldown (immediately before galvanizing); this time snapshot indicates the level of residual stress and strain in the detail produced by welding
t_5	5 s after dipping begins (liquid surface coincides with the crack path in the physical beam sample)
t_6	20 s after dipping begins (liquid surface at midbeam level)
t_7	37.5 s after dipping begins (liquid surface at the beam cope level)
t_8	20 s after the start of extraction (liquid surface at midbeam level)
t_9	40 s after the start of extraction (the point at which the beam has just been completely removed from the zinc)
t_{10}	50 s after the start of postgalvanizing cooldown
t_{11}	3,600 s after the start of postgalvanizing cooldown

Four weld sequences were simulated to study the effect of the welding sequence, as shown in **Fig. 7** with yellow arrows. In the control model (Sequence 1, **Fig. 7a**), weld lines were deposited downward at all sides, including Sides A, B, and the beam end. In Sequence 2 (**Fig. 7b**), the weld direction was reversed at the end, and, in Sequence 3 (**Fig. 7c**), the weld directions at Sides A and B were reversed such that they were both upward. All the weld directions in Sequence 4 (**Fig. 7d**) were upward, opposite those applied in the control model.

The magnitude of heat input was inversely proportional to the percentage of time taken to ramp the temperature to the prescribed torch temperature. Four levels of heat

Copyright by ASTM Int'l (all rights reserved); Wed Dec 4 09:43:32 EST 2019
Downloaded/printed by
Kansas University (Kansas University) pursuant to License Agreement. No further reproductions authorized.

FIG. 7 Welding sequences modeled in the parametric study: (a) Sequence 1 (control model), (b) Sequence 2, (c) Sequence 3, and (d) Sequence 4.

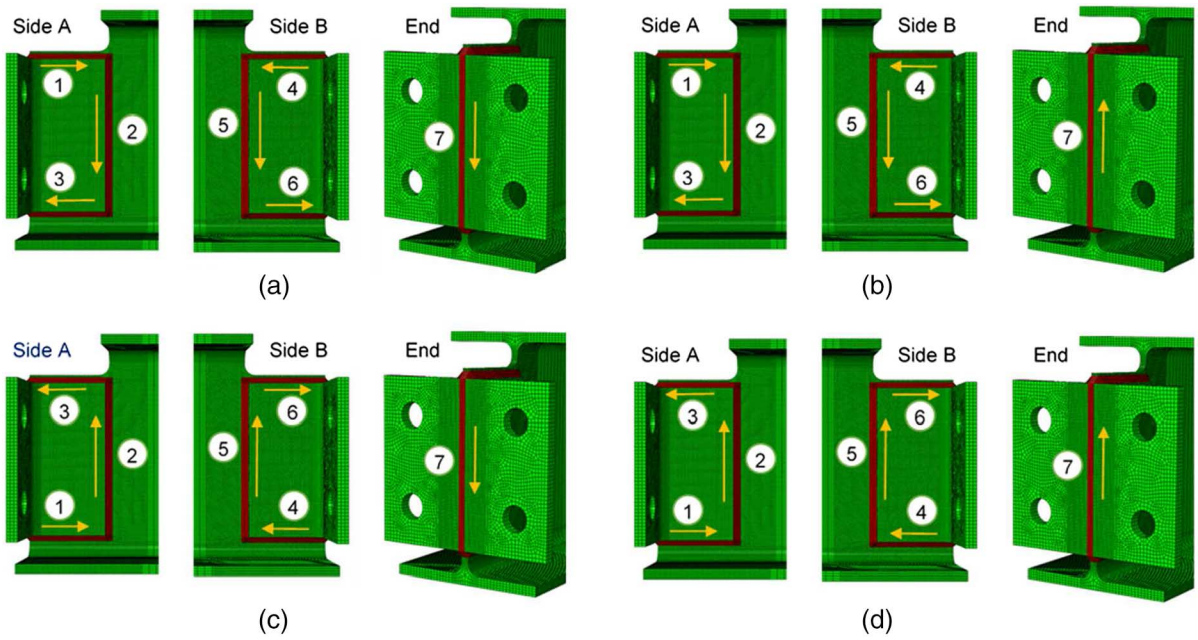

input were investigated in this study, as shown in Table 2. The heat input was calculated as the total thermal load reaction at the nodes on the boundary between weld elements and base metal, integrated over the corresponding time; this method has been verified by Dewees [27]. Total heat input depends on the temperature field at the liquid-solid boundary not the temperature of the interior of the weld pool [28]. Therefore, this numerical formulation for heat input is smaller than the real heat input put into the weld pool. Furthermore, the efficiency of welding equipment is normally around 50–70 %, so the nominal heat input measured with the welding equipment must be greater than the computed values [29]. For this reason, it is also valuable to consider the heat input magnitudes relative to each other, and the percent increase in heat input from that in the control model is shown in Table 2 as 13, 24, and 35 % for heat input levels 2, 3, and 4, respectively.

Three depths were considered for the double-angle connection in the parametric study: full depth of 140 mm, three-quarter depth of 105 mm, and half-depth of 70 mm (Fig. 8). These variations were chosen in order to investigate whether proximity

TABLE 2
Welding heat input in parametric study.

Model	Heat Input, J/mm	Heat Input, kJ/in.	Increase in Heat Input from Control Model, %
Heat input 1 (control model)	340	8.67	–
Heat input 2	390	9.78	13
Heat input 3	420	10.71	24
Heat input 4	460	11.69	35

Copyright by ASTM Int'l (all rights reserved); Wed Dec 4 09:43:32 EST 2019
Downloaded/printed by
Kansas University (Kansas University) pursuant to License Agreement. No further reproductions authorized.

FIG. 8 Change of connection depth in parametric study: (a) Depth 1 (control model; full-depth connection), (b) Depth 2 (three-quarters–depth connection), and (c) Depth 3 (half-depth connection).

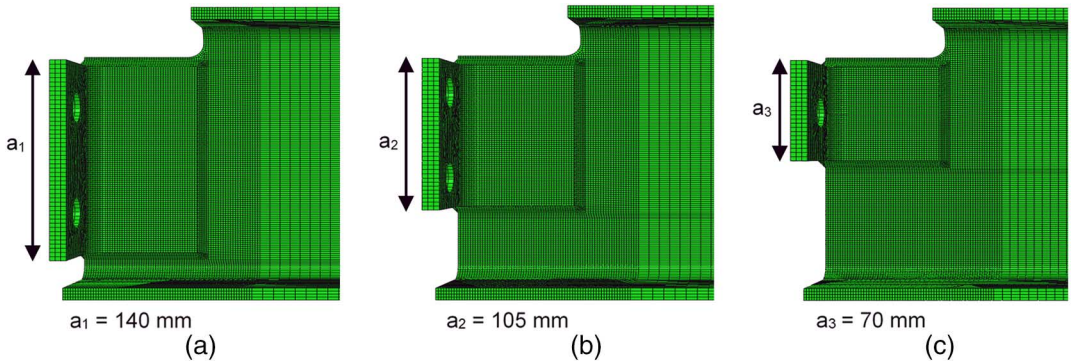

between the connection detail and the k-zone (the transition portion between the flange and web in a steel hot-rolled shape) had a significant effect on the stress and strain demands in that region.

Results and Discussion

Results for the control model are presented first to illustrate the general behavior during welding and galvanizing, followed by effects of welding sequence, heat input, and connection depth. Because the modeling approach is time dependent, results are shown for the entire model at discrete times t_1–t_{11}, as well as for selected points for the entire time history. Results are presented in terms of temperature (°C), von Mises stresses, and equivalent plastic strain (PEEQ).

PEEQ directly reflects the cumulative effect of the loading and unloading cycles, and thus was an important parameter for capturing this effect. In Abaqus [20], PEEQ is defined as follows:

$$\bar{\varepsilon}^{pl}|_0 + \int_0^t \dot{\bar{\varepsilon}}^{pl} dt \tag{1}$$

where ε^{pl} is the plastic strain, $\bar{\varepsilon}^{pl}|_0$ is the initial PEEQ, and $\dot{\bar{\varepsilon}}^{pl} = \sqrt{\frac{2}{3}\dot{\varepsilon}^{pl}\dot{\varepsilon}^{pl}}$.

This relationship shows the nature of PEEQ as a cumulative plastic strain measure.

Additionally, PEEQ used in conjunction with von Mises stresses has been established in the literature as an appropriate indicator to predict cracking potential [30–40]. Fracture problems are typically solved by invoking energy principles as crack propagation involves dissipation of energy. A crack is assumed to grow when the energy release rate is greater than a critical material-dependent value, which is a measure of the material's fracture toughness [41,42]. The strain energy density formulation in an elastic-plastic material, W, is dependent on the von Mises stress and PEEQ as follows:

$$W = \frac{1-2\nu}{6E}\sigma_{kk} + \frac{1+\nu}{3E}\sigma_{VM} + \int_0^t \sigma_{VM}\dot{\epsilon}^{pl} d\tau \tag{2}$$

Copyright by ASTM Int'l (all rights reserved); Wed Dec 4 09:43:32 EST 2019
Downloaded/printed by
Kansas University (Kansas University) pursuant to License Agreement. No further reproductions authorized.

$$W = \frac{1-2\nu}{6E}\sigma_{kk} + \frac{1+\nu}{3E}\sigma_{VM} + \sigma_{VM}\dot{\epsilon}^{pl} \quad (3)$$

where σ_{VM} is the von Mises effective stress, $\dot{\epsilon}^{pl}$ is the plastic strain rate, and ϵ^{pl} is the PEEQ. This strain energy density is used by the J-integral to calculate the energy release rate in a cracked body. Thus, von Mises and PEEQ are good indicators of possible crack locations.

CONTROL MODEL

Temperature Response of the Control Model

Fig. 9 presents the temperature distribution in the control model at times t_1–t_{11}; the figure also shows corresponding deformation patterns with a magnification factor of 50. It can be seen that the temperature during dipping (t_5–t_7) increased rapidly because of the high convective coefficient of the galvanizing bath (1,350 W/m^2/K), whereas temperatures during and immediately after extraction (t_8–t_{10}) slowly decreased because of the low convective coefficient for air (10 W/m^2/K). It is also apparent that the beam end with the welded connection cooled slower than the rest of the section because of its greater thickness.

Fig. 10 presents temperature history at two points in the beam, A and B. Point A is located at a distance of 1.1 mm from the weld toe, near the k-zone, while Point B is approximately 3.5 mm from the weld toe. Point A corresponds to the location of the crack in the physical beam sample, and Point B captures behavior in the cope region, which is also susceptible to cracking during galvanization [43]. The temperature history was similar for both points. Both curves exhibited multiple peaks during the welding process as the different weld passes were made and a near-instantaneous spike in temperature occurred upon dipping. The one-hour cooldown periods postwelding and postgalvanizing were sufficient to return the beam nearly to room temperature (20°C).

Stress Response of the Control Model

Fig. 11 presents the von Mises stress field for times t_1–t_{11}. Weld-induced stresses at times t_1–t_3, during welding and cooldown after welding, were very large at areas around the deposited welds, particularly along the crack path and the beam cope. These stresses exceeded the yield strength at room temperature (345 MPa) and greatly exceeded the yield strength at higher temperatures.

The stress pattern at t_4 shows the residual stresses induced by the welding process. These welding residual stresses dramatically changed when the beam detail was subjected to the galvanizing process, especially during the dipping stage. During this time, the beam distorted as the bottom portion expanded while it was submerged in the molten zinc and the top portion was still exposed to air [44]. This uneven expansion created a bending deformation in the beam section, as shown in times t_5–t_7. There were different thermal gradients between the elements above and below the level of the simulated liquid surface, which generated high local stresses in the longitudinal direction on elements above the surface. At times at t_5–t_7, large stresses of 320–360 MPa appeared in the vicinity of the physical crack path, at midbeam, and at the beam cope. During the dwell time, the difference between thermal gradients in the beam decreased, which reduced distortion and relieved stresses throughout the beam assembly. At t_8 and t_9, stresses were redistributed and reduced to magnitudes less than 200 MPa in most parts of the beam. At the beginning of the postgalvanizing cooldown, stresses again increased because of the differential cooling rate between the beam and the connection detail. Finally, stresses

Copyright by ASTM Int'l (all rights reserved); Wed Dec 4 09:43:32 EST 2019
Downloaded/printed by
Kansas University (Kansas University) pursuant to License Agreement. No further reproductions authorized.

FIG. 9 Temperature field (°C) and deformed shape of the control model (amplified 50×) at discrete points of time throughout the welding and galvanizing processes, as defined in **Fig. 5** and **Fig. 6**.

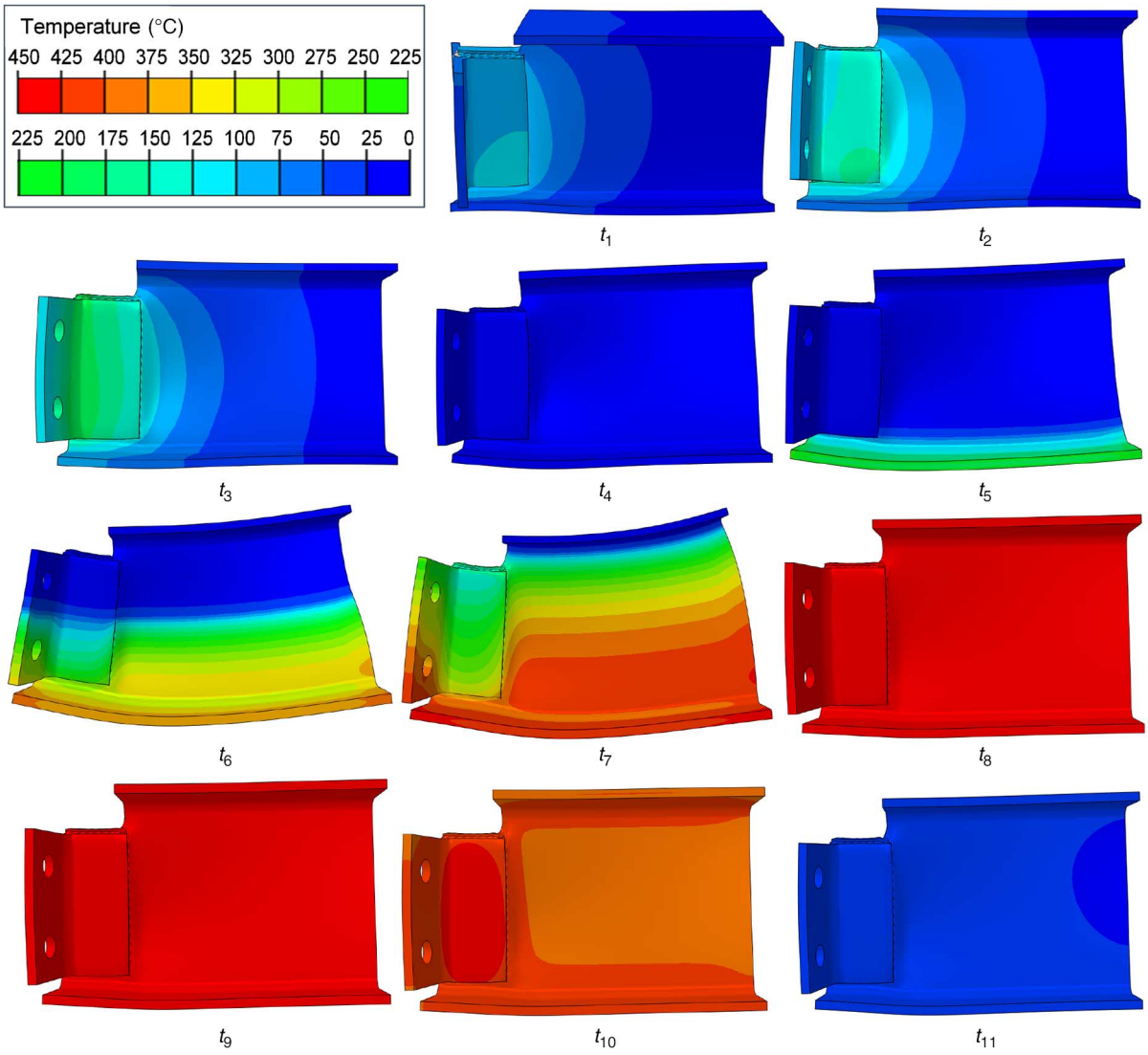

approached steady-state at time t_{11} when temperature in the beam had decreased to near room temperature.

Although cracking was not observed at the beam cope in the physical beam sample, model results showed that this area sustained high stress demands multiple times during the processes. Cope cracking in structural steel after galvanizing has been reported in literature since the 1990s, with cracks found at flame-cut copes, extending radially at 45° [43]. A research project was conducted by researchers at CANMET Materials Technology Laboratory (Hamilton, Ontario, Canada) to address this problem, concluding that the cause of cope cracking was the combination of stress demands and a susceptible material [45]. While material susceptibility is not part of the scope of the present study, this modeling effort has shown that stress demands are high at the cope area during the

Copyright by ASTM Int'l (all rights reserved); Wed Dec 4 09:43:32 EST 2019

Downloaded/printed by
Kansas University (Kansas University) pursuant to License Agreement. No further reproductions authorized.

FIG. 10 Temperature history at Point A (at crack opening) and Point B (at beam cope).

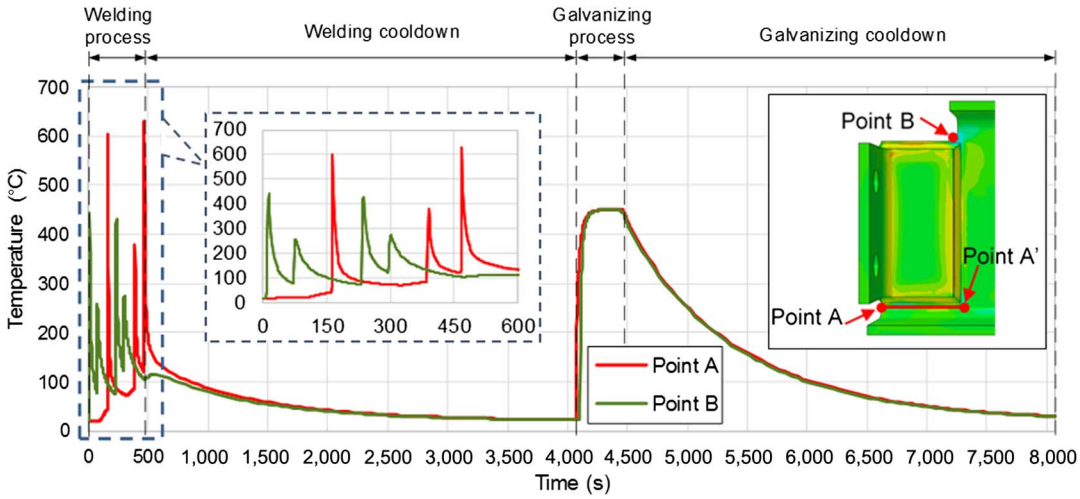

FIG. 11 Von Mises stress (MPa) in the control model throughout the welding and galvanizing processes, at times defined in Fig. 5 and Fig. 6.

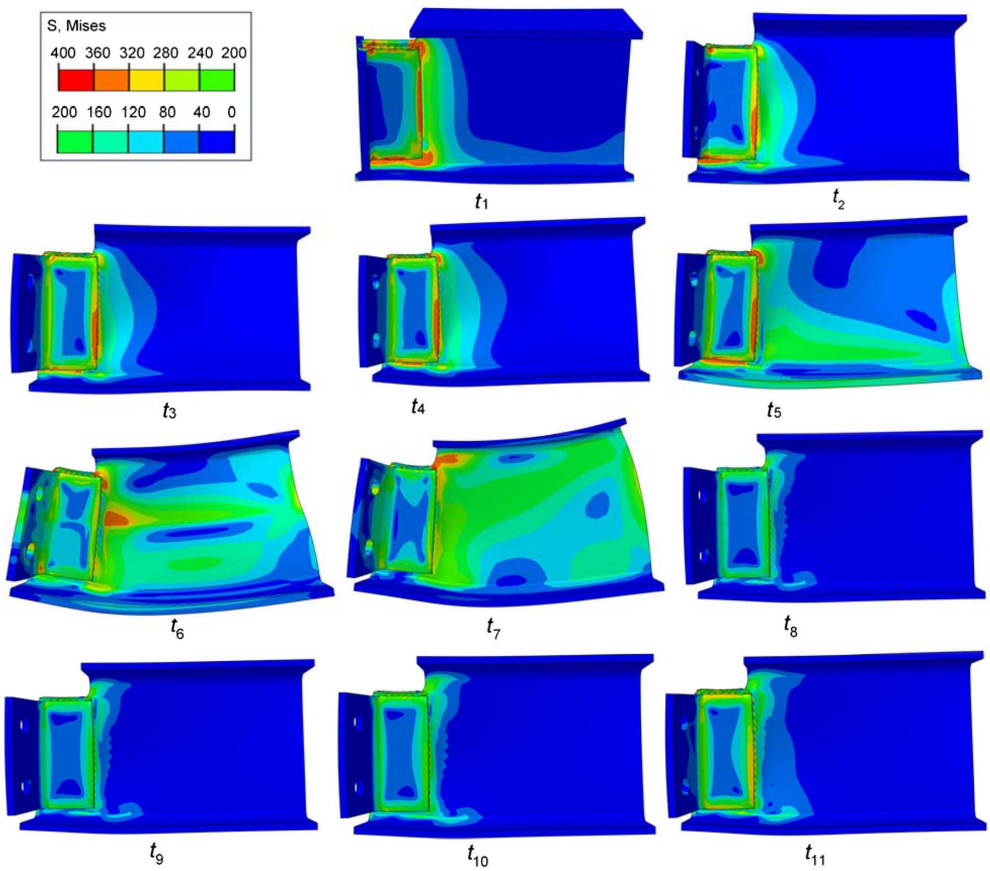

Copyright by ASTM Int'l (all rights reserved); Wed Dec 4 09:43:32 EST 2019
Downloaded/printed by
Kansas University (Kansas University) pursuant to License Agreement. No further reproductions authorized.

dipping process. ASTM A143, *Standard Practice for Safeguarding Against Embrittlement of Hot-Dip Galvanized Structural Steel Products and Procedure for Detecting Embrittlement* [46], specifies a minimum cope radius of 25 mm, so the cope radius of 10 mm used in this study is smaller than permitted by this specification. The effect of cope radius on stress demand is a topic for future research.

The stress history is presented in Fig. 12 for Points A and B on the beam. Both Points A and B were subjected to loading and unloading cycles throughout the welding and galvanizing processes. As is evident from Fig. 12a, stresses at Point A and Point B fluctuated dramatically during welding and dipping, repeatedly exceeding the yield strength. While Point A sustained only one large spike in stress during dipping, Point B sustained three spikes in the beam cope, as shown in Fig. 12c. The spike in stresses at Point A was caused by the combination of global bending and local distortion when the area surrounding Point A was submerged into the zinc bath. This effect also created the first spike at Point B. The

FIG. 12 Von Mises stress history at Point A (at crack opening area) and Point B (beam cope area), as defined in Fig. 10: (a) whole processes, (b) detailed view during welding, and (c) detailed view during dipping.

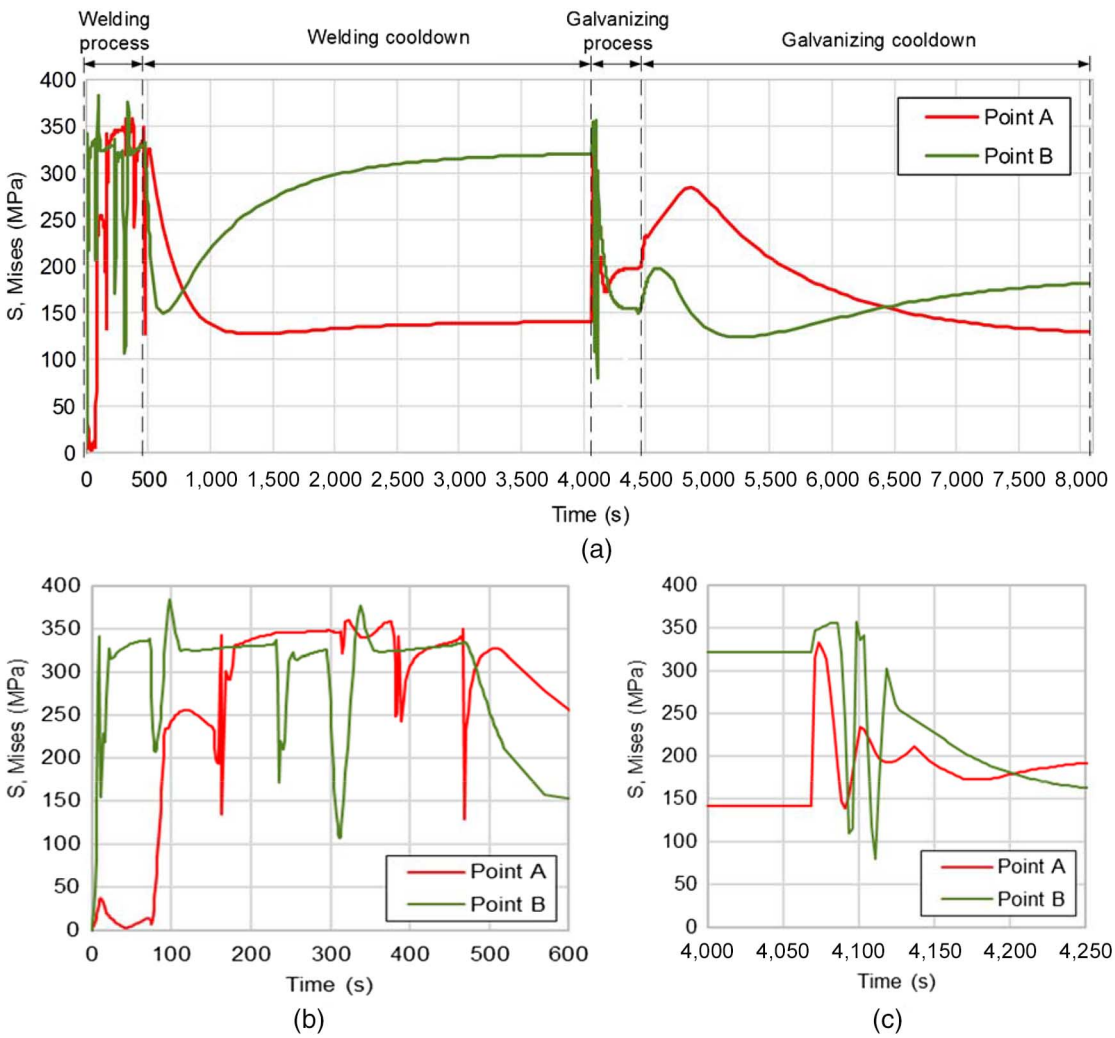

Copyright by ASTM Int'l (all rights reserved); Wed Dec 4 09:43:32 EST 2019
Downloaded/printed by
Kansas University (Kansas University) pursuant to License Agreement. No further reproductions authorized.

second spike at Point B occurred when the simulated liquid surface reached the level of the beam cope, producing localized distortion. The third spike at Point B developed after the beam was completely submerged, and constraint produced severe tension in the cope.

Stresses along path A-A' (Fig. 10) were found to be very high during welding (t_1–t_4) and in the early stages of galvanizing (t_5) around the yield strength of the material (345 MPa). After the simulated liquid zinc surface surpassed the level of path A-A' (at time t_5), stresses decreased dramatically to magnitudes varying from 50–150 MPa along the path for times t_8 and t_9. Finally, stresses on the path increased slightly again during postgalvanizing cooldown (t_{10} and t_{11}), varying between 75–225 MPa.

The phenomenon of decreasing stresses during hot-dip galvanizing has been mentioned many times in the literature. Minami and Horikawa [47,48] and Mori, Minami, and Horikawa [49] stated that hot-dip galvanizing reduces stresses because of an annealing effect and the transmission of stresses from the weld toe area to the newly formed zinc layer. In addition, in ASTM A143 [46] it is stated that "As the sheet or plate is heated to galvanizing temperature, 820°F to 850°F (438°C to 454°C), the stress can be slightly relieved but the constraint of the framing does not allow the stresses to be completely relieved." Such statements do not readily acknowledge that a structural component could be subjected to a significant stress-increasing state before reaching a stress-relieving state, which may be extremely influential in the development of cracking during galvanizing.

Strain Response of the Control Model

Stresses near the connection detail exceeded the yield strength of the material multiple times because of the loading and unloading cycles experienced during welding and galvanizing processes. Because of this loading and unloading process, plastic deformations were significant.

Fig. 13 presents the PEEQ field for times t_1–t_{11}. At times t_1–t_3, the welding process induced PEEQs on the base metal at locations around the welds. After the first round of welds on Side A (Welds 1, 2, and 3 in Fig. 5), the maximum PEEQ value was 12.6 % and increased to 13.1 % after finishing the weld at the beam end (Weld 7 in Fig. 5). At this point, the location of maximum PEEQ value moved from the lower right corner to the lower left corner of the angle on Side A.

When the beam was dipped into the galvanizing bath, the PEEQ field developed over a wider influence area, and the maximum value increased to 14.1 %, as shown at t_5–t_7. The spread of the strain field was prominent at the area of the beam cope and the crack path A-A'. Although the maximum value increased, the magnitude of the increase did not reflect the overall change of PEEQ during the hot-dip galvanizing process. From dwelling to postgalvanizing cooldown, the change in PEEQ was small, as shown at t_8–t_{11}. In general, the hot-dip galvanizing process produced smaller plastic strains on the beam than the welding process, although the additional plastic strains could still play an important role regarding the critical condition of the as-welded detail.

Strain behavior can also be observed in Fig. 14, which depicts the PEEQ history at Points A and B. Note that Point A is at a distance of 1.1 mm from the point where the maximum value of PEEQ occurs in the crack opening area, while Point B is at the point with maximum PEEQ at the cope (Fig. 15). The majority of the increase in PEEQ can be attributed to the cooling stages after nearby weld passes. For example, PEEQ at Point A increased significantly during cooling after Welds 3, 6, and 7 were placed. The detail also experienced a large increase in PEEQ during the dipping stage. PEEQ magnitudes at Point A were approximately 50 % higher than at Point B. When PEEQs were examined along the

Copyright by ASTM Int'l (all rights reserved); Wed Dec 4 09:43:32 EST 2019
Downloaded/printed by
Kansas University (Kansas University) pursuant to License Agreement. No further reproductions authorized.

FIG. 13 Evolution of PEEQ in the control model at points of time throughout the welding and galvanizing processes defined in **Fig. 5** and **Fig. 6**.

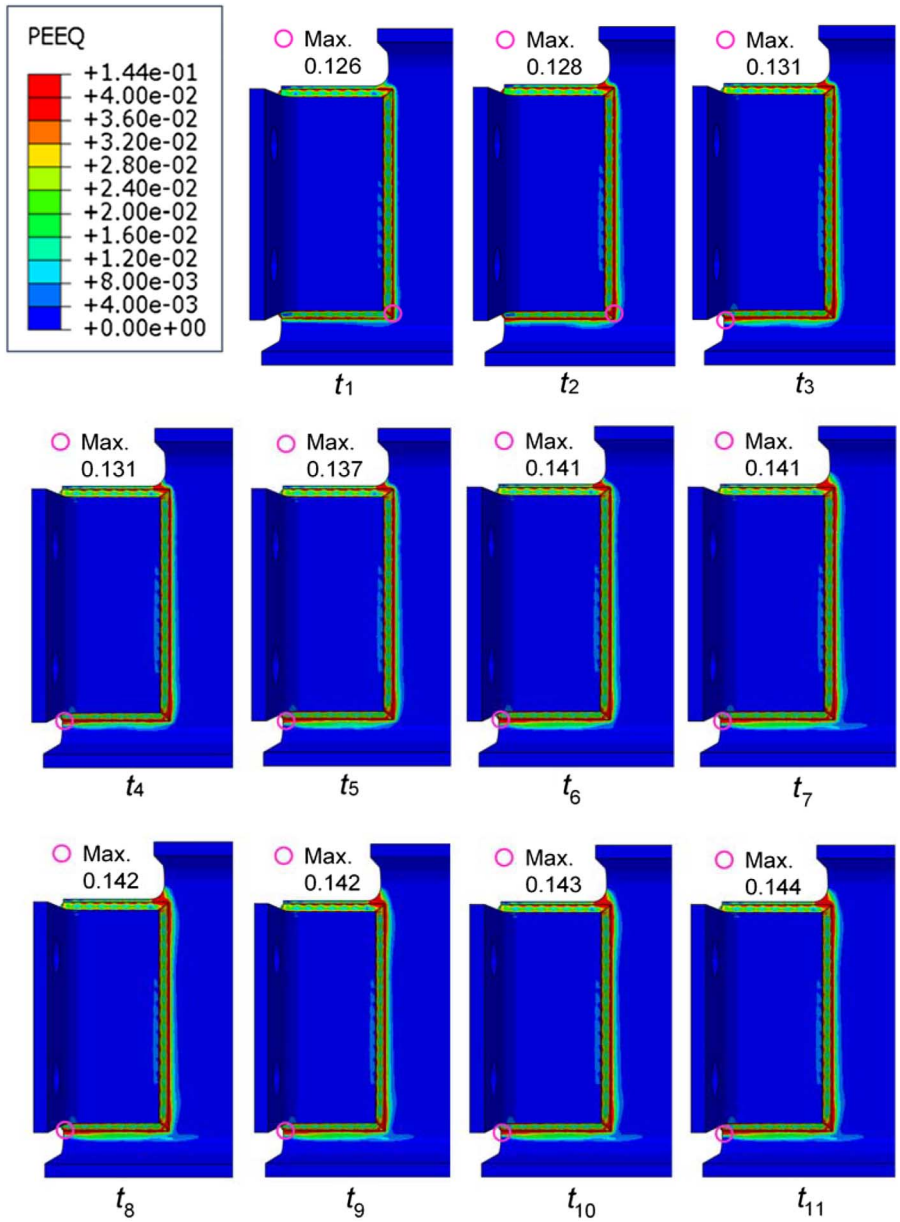

crack path, it was found that the region surrounding Point A (the region in the physical beam sample that cracked) experienced the largest PEEQ values.

Relationship between Stress and Strain Fields and Location of the Observed Crack

From these results, it is concluded that the combined welding and galvanizing processes generated high strain demands at multiple locations near the connection, including at the

Copyright by ASTM Int'l (all rights reserved); Wed Dec 4 09:43:32 EST 2019
Downloaded/printed by
Kansas University (Kansas University) pursuant to License Agreement. No further reproductions authorized.

FIG. 14 PEEQ history at Point A (at crack opening area) and Point B (beam cope area), as defined in **Fig. 10**.

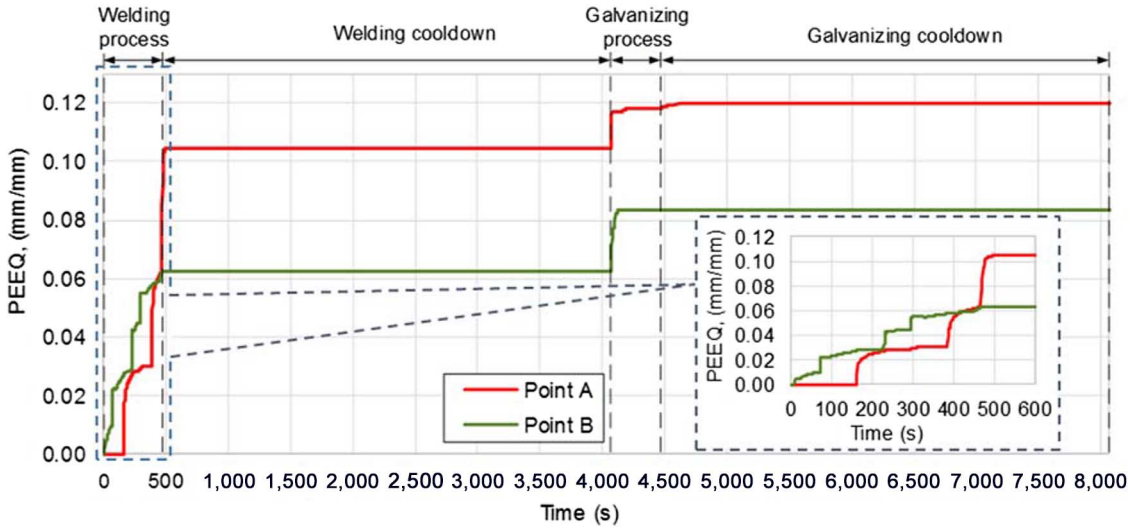

FIG. 15

PEEQ from the control model at time t_9.

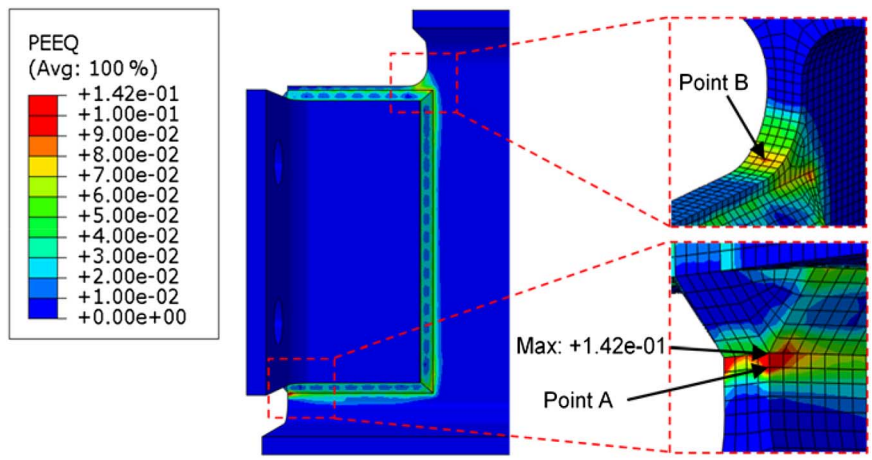

crack path. In fact, the area containing the maximum PEEQ (14.2 %) was coincident with the opening region of the actual crack path, as shown in **Fig. 13** and **Fig. 15**. While the simulations indicate that this is an important factor, it is not conclusive that high strains were the single most important factor contributing to the initiation and development of the observed crack, and it is readily acknowledged that there are many other factors that could have played a role in the initiation of the crack.

Research conducted by Rudd et al. [8] has shown that strain resistance depends significantly on the chemical composition of the zinc bath, and PEEQ strain resistance could vary as much as from 5 to 30 %. Among additives, tin was believed to have had the greatest negative influence on the ability of steel material to strain.

Copyright by ASTM Int'l (all rights reserved); Wed Dec 4 09:43:32 EST 2019
Downloaded/printed by
Kansas University (Kansas University) pursuant to License Agreement. No further reproductions authorized.

There are also another three factors that could contribute to the occurrence of the observed crack. The first factor is possible increased hardness at the heat-affected zone [50,51], which would be expected to reduce the material resistance to failure. The second factor is the effect of rolling, which introduces additional residual stresses and strains and potentially poor mechanical properties at the k-zone [52–54] because of cold-working and associated hardening. The third factor is the possible presence of welding defects, which can accelerate crack formation [50,55].

Influence of the Welding Simulation on the Model Response

To examine the effect of neglecting the welding process on the simulation results, a model was created that was identical to the control model, except that the welding procedures were omitted. The angles and weld elements were attached to the steel beam as one part, and the model was subjected to the galvanizing process. A comparison between the control model and the identical model that did not include welding is shown in Fig. 16 and Fig. 17.

The difference in calculated stress and strain between the two approaches is quite striking. In the case for which the welding process was neglected, stresses at the end of the galvanizing sequence were not strongly affected, but PEEQ magnitudes were

FIG. 16 (a) Von Mises stress history across the galvanizing process predicted by finite element simulations with and without welding procedure, (b) von Mises stresses at t_4 (without explicit weld modeling), (c) von Mises stresses at t_4 (with explicit weld modeling), (d) von Mises stresses at t_{11} (without explicit weld modeling), and (e) von Mises stresses at t_{11} (with explicit weld modeling).

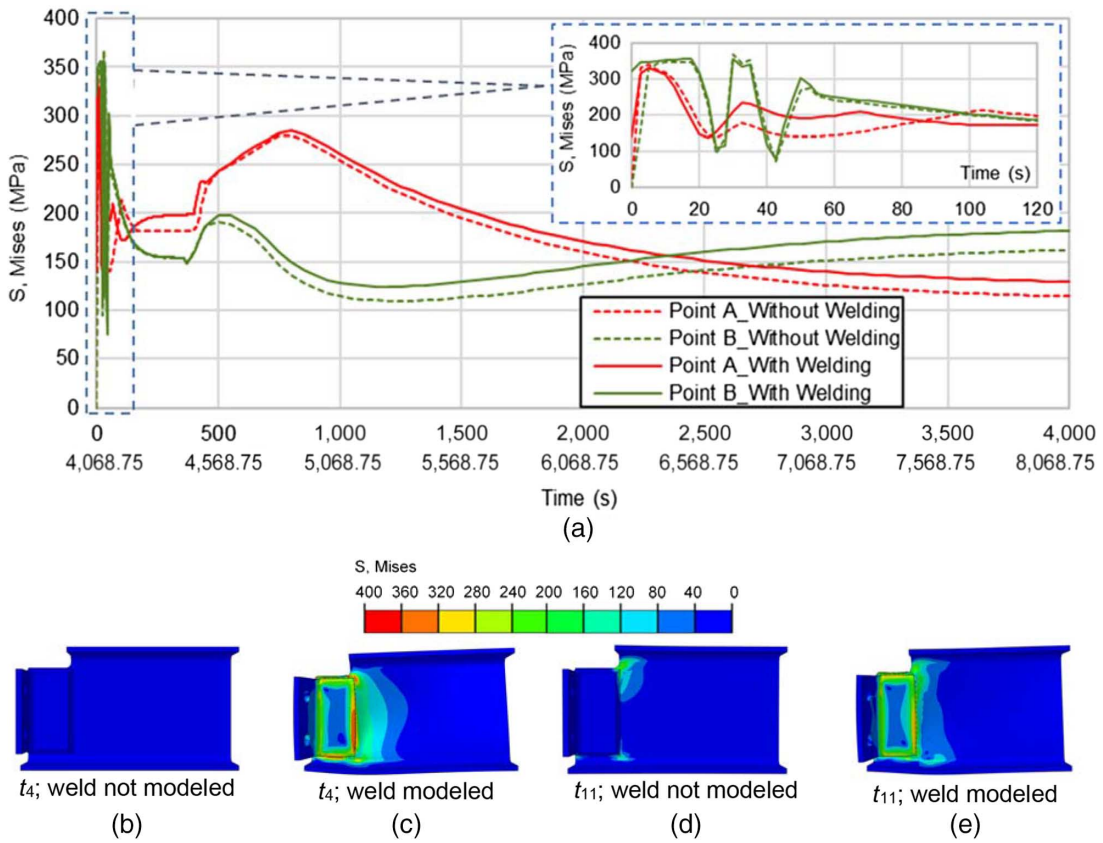

Copyright by ASTM Int'l (all rights reserved); Wed Dec 4 09:43:32 EST 2019
Downloaded/printed by
Kansas University (Kansas University) pursuant to License Agreement. No further reproductions authorized.

FIG. 17 (a) Comparison of PEEQ history across the galvanizing process predicted by finite element simulations with and without welding procedure, (b) PEEQ at t_4 (without explicit weld modeling), (c) PEEQ at t_4 (with explicit weld modeling), (d) PEEQ at t_{11} (without explicit weld modeling), and (e) PEEQ at t_{11} (with explicit weld modeling).

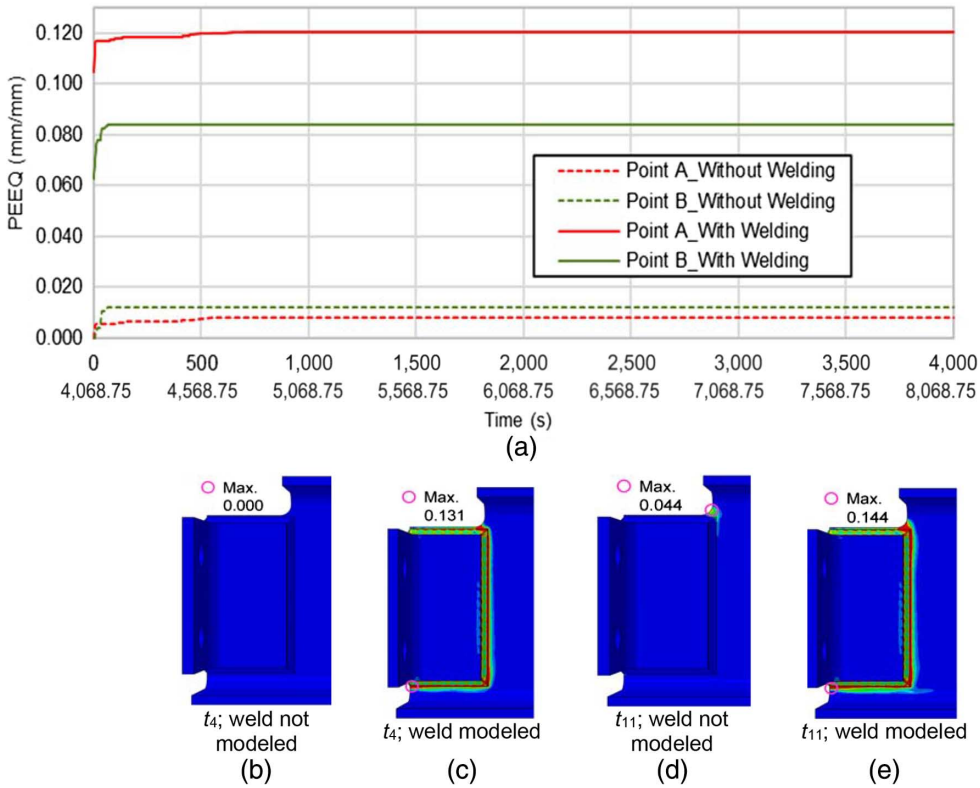

severely underestimated. This is an important consideration because PEEQ appears to have provided a better prediction of the observed crack path than stress in this case.

RESULTS OF THE PARAMETRIC STUDY

Effect of Welding Sequence

Fig. 18 presents PEEQ for the models in which the welding sequence was varied. Times t_4 and t_9 show behavior immediately before and after galvanizing, respectively. Reversing the direction of Weld 7 at the beam end helped to somewhat reduce the maximum value of PEEQ, from 14.2 to 13.5 %, while welding sequences 3 and 4 resulted in further reduction in PEEQ to 13.0 %. It is also interesting to note that welding sequences 3 and 4 relocated the critical point from the observed crack opening area to the beam cope area. In general, high strains developed near regions of weld termination. Therefore, it is recommended to avoid weld termination in sensitive areas. Among the sequences studied, welding sequences 3 and 4 provided the most favorable results. It can be expected that a different dipping orientation would yield different results, so it is simply noted that welding sequence did have a significant effect on the magnitudes of strain at sensitive locations.

Copyright by ASTM Int'l (all rights reserved); Wed Dec 4 09:43:32 EST 2019
Downloaded/printed by
Kansas University (Kansas University) pursuant to License Agreement. No further reproductions authorized.

FIG. 18 Distribution of PEEQ before and after galvanizing when changing welding sequence: (a) Sequence 1 (control model), (b) Sequence 2, (c) Sequence 3, and (d) Sequence 4.

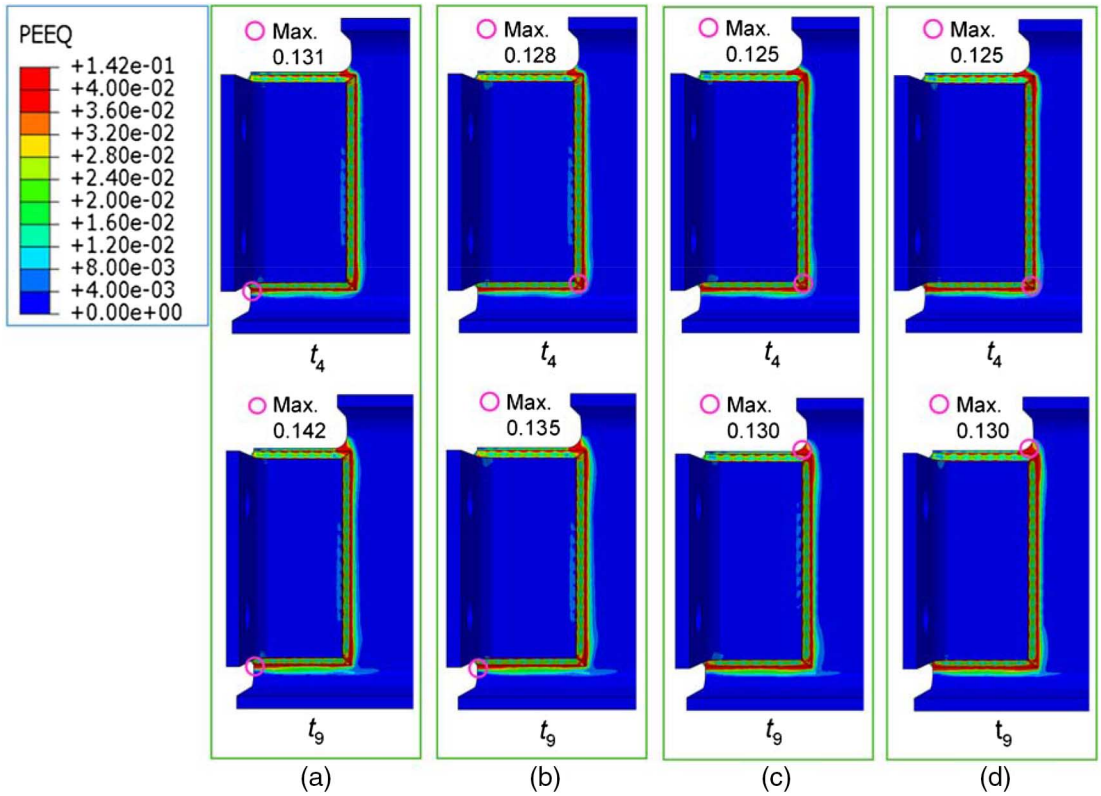

FIG. 19 Effect of heat input on PEEQ history at Point A.

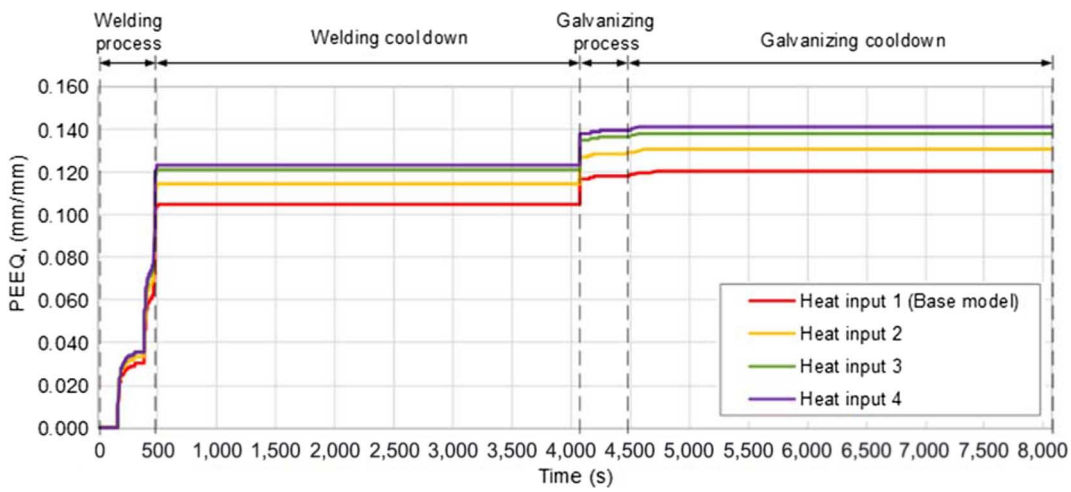

Copyright by ASTM Int'l (all rights reserved); Wed Dec 4 09:43:32 EST 2019

Downloaded/printed by
Kansas University (Kansas University) pursuant to License Agreement. No further reproductions authorized.

FIG. 20

Distribution of PEEQ before and after galvanizing when changing welding angle depth: (a) Depth 1(control model), (b) Depth 2, and (c) Depth 3.

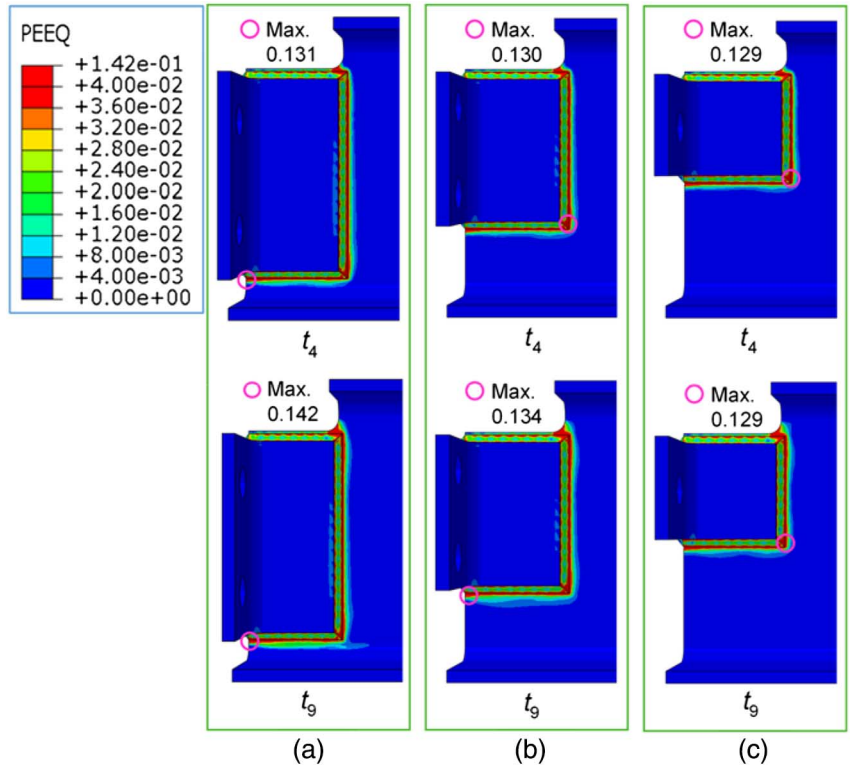

It is further noted that inelastic strains accumulated with the introduction of each new weld pass into the connection. Thus, it is recommended to minimize the number of welds to the greatest extent possible when using welded connections that will be galvanized.

Effect of Welding Heat Input

It was found that greater levels of heat input corresponded with greater maxima of PEEQ, although the relationship was not linearly proportional, as shown in Fig. 19. It is also interesting to note that the increase in welding heat input did not change the location of the area experiencing the maximum value of PEEQ (Point A).

Effect of Connection Depth

Fig. 20 shows that moving the connection away from the k-zone of the beam section helped reduce the maximum value of PEEQ. By removing the connection weld from the k-zone, the weld was removed from the vicinity of restraint imposed by the bottom flange as well as from the stress concentration formed by the fillet. While not a factor that was captured in the analyses, it should be noted that removing the connection from the k-zone also removes the weld from a region with high rolling stresses [56] and material hardening. Using the same reasoning, removing the connection a distance from the cope could also help to isolate the weld from deleterious interactions with hardened material and stress concentrations.

Copyright by ASTM Int'l (all rights reserved); Wed Dec 4 09:43:32 EST 2019
Downloaded/printed by
Kansas University (Kansas University) pursuant to License Agreement. No further reproductions authorized.

Conclusions

The following conclusions were drawn from this study:

(1) The connection detail sustained many cycles of loading and unloading throughout welding and galvanizing, which generated high stresses and strains, especially in the area coinciding with the bottom weld of the connection (location of observed cracking in the physical sample) and the beam cope.
(2) The welding process generated high strain demands at the weld toe in the area surrounding the connection. The galvanizing process introduced additive inelastic strains that occurred over a larger affected area. The inelastic strains induced by galvanizing were smaller than those produced by welding, but they were significant.
(3) If the connection detail was fabricated with the welding sequence simulated in the control model of this study (the actual welding sequence is unknown), the area at the opening of the observed crack path would be the most critical area on the connection detail in terms of the accumulation of plastic strain.
(4) To reduce the susceptibility to cracking during galvanizing of components, such as the beam evaluated in this study, it is recommended to:
   – Ensure that welds are terminated away from locations of geometric restraint or severe stress concentrations
   – Decrease welding heat input as much as possible
   – Ensure that the connection is not placed close to the k-zone of the beam. In this study, it was shown that by removing the weld from that region of restraint and stress concentration the strains could be reduced. An additional benefit to removing the connection from that area is minimizing interactions with rolling residual stresses and hardened material.

Although the results of this study showed that the combined strains introduced by welding and hot-dip galvanizing processes were very high in the area coinciding with the observed crack path, the reader is cautioned against making strong conclusions regarding the direct cause of the cracking. Cracking is believed to be dependent upon interaction with other parameters (steel chemistry, galvanizing composition, dipping angle and speed, etc.), which makes this an extremely complex problem. Nonetheless, by examining the relative influence of heat input, welding sequence, and connection depth, some key observations were made that should serve to better enable engineers, fabricators, and galvanizers to create welded details less susceptible to cracking during galvanizing. Additionally, the modeling methodology used in this study has provided an approach for explicitly accounting for the influence of welding on the behavior of steel components during galvanizing, which was found to have a very strong influence on calculated strains.

References

[1] Koch, G., Brongers, M., Thompson, N., Virmani, P., and Payer, J., "Corrosion Costs and Preventive Strategies in the United States," Report No. FHWA-RD-01-156, U.S. Department of Transportation, Washington, DC, 2002, 12p.
[2] Chen, T.-T. and Hsu, Y. T., "Study on Hot-Dip Galvanized Steel Bridges for Life-Cycle Cost Model," presented at the *International Conference on Sustainable Civil Infrastructure*, Hubei, China, July 20–22, 2014, ASCE, Reston, VA, pp. 141–149.
[3] Feldmann, M., Pinger, T., Schäfer, D., Pope, R., Smith, W., and Sedlacek, G., *Hot-Dip-Zinc-Coating of Prefabricated Structural Steel Components*, JRC Scientific and

Copyright by ASTM Int'l (all rights reserved); Wed Dec 4 09:43:32 EST 2019
Downloaded/printed by
Kansas University (Kansas University) pursuant to License Agreement. No further reproductions authorized.

Technical Reports, Office for Official Publications of the European Communities, Luxembourg, 2010, 110p.
[4] Kinstler, T. J., "Current Knowledge of the Cracking of Steels during Galvanizing," GalvaScience LLC, AISC, Chicago, IL, 2005, 79p.
[5] Toi, Y., Kobashi, K., and Iezawa, T., "Finite Element Analysis of Thermal Elasto Plastic Behaviours of Bridge Girders in Hot Dip Galvanization," *Comput. Struct.*, Vol. 53, No. 6, 1994, pp. 1307–1316, https://doi.org/10.1016/0045-7949(94)90398-0
[6] Toi, Y. and Lee, J.-M., "Thermal Elasto-Viscoplastic Damage Behavior of Structural Members in Hot-Dip Galvanization," *Int. J. Damage Mech.*, Vol. 11, No. 2, 2016, pp. 171–185, https://doi.org/10.1106/105678902023083
[7] Kleineck, J. R., "Galvanizing Crack Formation at Base Plate to Shaft Welds of High Mast Illumination Poles," M.S. thesis, University of Texas at Austin, Austin, TX, 2011.
[8] Rudd, W. J., Wen, S. W., Langenberg, P., Donnay, B., Voelling, A., Pinger, T., Feldmann, M., Carpio, J., Casado, J. A., Alvarez, J. A., and Gutierrez-Solana, F., *Failure Mechanisms during Galvanizing*, Office for Official Publications of the European Communities, Luxembourg, 2008, 141p.
[9] Deng, D. and Murakawa, H., "Prediction of Welding Distortion and Residual Stress in a Thin Plate Butt-Welded Joint," *Comput. Mater. Sci.*, Vol. 43, No. 2, 2008, pp. 353–365, https://doi.org/10.1016/j.commatsci.2007.12.006
[10] Perić, M., Tonković, Z., Rodić, A., Surjak, M., Garašić, I., Boras, I., and Švaić, S., "Numerical Analysis and Experimental Investigation of Welding Residual Stresses and Distortions in a T-Joint Fillet Weld," *Mater. Des.*, Vol. 53, 2014, pp. 1052–1063, https://doi.org/10.1016/j.matdes.2013.08.011
[11] Keinänen, H., "Computation of Residual Stresses for a Repair Weld Case," *Weld. World*, Vol. 60, No. 3, 2016, pp. 507–513, https://doi.org/10.1007/s40194-016-0323-y
[12] Joosten, M. M. and Gallegillo, M. S., "A Study of the Effect of Hardening Model in the Prediction of Welding Residual Stress," presented at the *ASME 2012 Pressure Vessels and Piping Conference*, Toronto, Canada, July 15–19, 2012, Pressure Vessels and Piping Division, ASME, New York, NY, pp. 1045–1054.
[13] Xu, J. J., Gilles, P., and Duan, Y. G., "Simulation and Validation of Welding Residual Stresses Based on Non-Linear Mixed Hardening Model," *Strain*, Vol. 48, No. 5, 2012, pp. 406–414, https://doi.org/10.1111/j.1475-1305.2012.00836.x
[14] Dewees, D., Prueter, P., and Kummari, S., "A Continued Evaluation of The Role of Material Hardening Behavior for the NeT TG1 and TG4 Specimens," presented at the *ASME 2014 Pressure Vessels and Piping Conference*, Anaheim, CA, July 20–24, 2014, Pressure Vessels and Piping Division, ASME, New York, NY, 12p.
[15] Håkansson, P., Wallin, M., and Ristinmaa, M., "Comparison of Isotropic Hardening and Kinematic Hardening in Thermoplasticity," *Int. J. Plast.*, Vol. 21, No. 7, 2005, pp. 1435–1460, https://doi.org/10.1016/j.ijplas.2004.07.002
[16] Mullins, J. and Gunnars, J., *Influence of Hardening Model on Weld Residual Stress Distribution, Report No. 2009:16*, Inspecta Technology AB, Stockholm, Sweden, 2009, 44p.
[17] Lindgren, L.-E., "Finite Element Modeling and Simulation of Welding Part 1: Increased Complexity," *J. Therm. Stresses*, Vol. 24, No. 2, 2001, pp. 141–192, https://doi.org/10.1080/01495730150500442
[18] Lindgren, L.-E., "Finite Element Modeling and Simulation of Welding. Part 2: Improved Material Modeling," *J. Therm. Stresses*, Vol. 24, No. 3, 2001, pp. 195–231, https://doi.org/10.1080/014957301300006380
[19] Lindgren, L.-E., "Numerical Modelling of Welding," *Comput. Meth. Appl. Mech. Eng.*, Vol. 195, Nos. 48–49, 2006, pp. 6710–6736, https://doi.org/10.1016/j.cma.2005.08.018
[20] Simulia, D. S., "Abaqus 2017," *Abaqus 2017*, Simulia, Editor, Dassault Systèmes, Johnston, RI, 2017.
[21] Simulia, "Abaqus Welding Interface (AWI)—User's Manual," 2017.
[22] Shubert, M., Pandheeradi, M., Arnold, F., and Habura, C., "An Abaqus Extension for Welding Simulations," presented at the *2010 SIMULIA Customer Conference*, Providence, RI, May 25–27, 2010, Dassault Systèmes, Johnston, RI, 2010, 15p.

Copyright by ASTM Int'l (all rights reserved); Wed Dec 4 09:43:32 EST 2019
Downloaded/printed by
Kansas University (Kansas University) pursuant to License Agreement. No further reproductions authorized.

[23] Malik, A. M., Qureshi, E. M., Dar, N. U., and Khan, I., "Analysis of Circumferentially Arc Welded Thin-Walled Cylinders to Investigate the Residual Stress Fields," *Thin Walled Struct.*, Vol. 46, No. 12, 2008, pp. 1391–1401, https://doi.org/10.1016/j.tws.2008.03.011

[24] Dal, M., Le Masson, P., and Carin, M., "A Model Comparison to Predict Heat Transfer during Spot GTA Welding," *Int. J. Therm. Sci.*, Vol. 75, 2014, pp. 54–64, https://doi.org/10.1016/j.ijthermalsci.2013.07.013

[25] Nguyen, K., Nasouri, R., Bennett, C., Matamoros, A., Li, J., and Montoya, A., "Sensitivity of Predicted Temperature in a Fillet Weld T-Joint to Parameters Used in Welding Simulation with Prescribed Temperature Approach," presented at the *Science in the Age of Experience*, Chicago, IL, May 15–18, 2017, Dassault Systèmes, Johnston, RI, pp. 232–247.

[26] Cresdee, R. B., Edwards, W. J., Thomas, P. J., and Voss, G. F., "Analysis of Beam Distortion during Hot Dip Galvanising," *Mater. Sci. Technol.*, Vol. 9, No. 2, 2013, pp. 161–162, https://doi.org/10.1179/mst.1993.9.2.161

[27] Dewees, D., "Verification of Welding Power Input in Two-Dimensional Welding Simulation," presented at the *ASME Verification and Validation Symposium*, Las Vegas, NV, May 2–4, 2012, ASME, New York, NY.

[28] Goldak, J. and Akhlaghi, M., *Computational Welding Mechanics*, Springer US, New York, NY, 2005, 322p.

[29] Attarha, M. J. and Sattari-Far, I., "Study on Welding Temperature Distribution in Thin Welded Plates through Experimental Measurements and Finite Element Simulation," *J. Mater. Process. Technol.*, Vol. 211, No. 4, 2011, pp. 688–694, https://doi.org/10.1016/j.jmatprotec.2010.12.003

[30] Wei, Z., Luo, L., Lin, B., Yang, F., Konson, D., Ellinghaus, K., Pieszkalla, M., Avery, K., Pan, J., and Engler-Pinto, C. C., "Hold-Time Effect on Thermo-Mechanical Fatigue Life and Its Implications in Durability Analysis of Components and Systems," *Mater. Perform. Charact.*, Vol. 4, No. 2, 2014, pp. 198–217, https://doi.org/10.1520/MPC20140032

[31] Banerjee, D., Iadicola, M., Creuziger, A., and Foecke, T., "Finite Element Modeling of Deformation Behavior of Steel Specimens under Various Loading Scenarios," *Key Eng. Mater.*, Vols. 651–653, 2015, pp. 969–974, https://doi.org/10.4028/www.scientific.net/KEM.651-653.969

[32] Xue, L., "Damage Accumulation and Fracture Initiation in Uncracked Ductile Solids Subject to Triaxial Loading," *Int. J. Solids Struct.*, Vol. 44, No. 16, 2007, pp. 5163–5181, https://doi.org/10.1016/j.ijsolstr.2006.12.026

[33] Faleskog, J. and Barsoum, I., "Tension–Torsion Fracture Experiments—Part I: Experiments and a Procedure to Evaluate the Equivalent Plastic Strain," *Int. J. Solids Struct.*, Vol. 50, Nos. 25–26, 2013, pp. 4241–4257, https://doi.org/10.1016/j.ijsolstr.2013.08.029

[34] Li, M., Barrett, R. A., Scully, S., Harrison, N. M., Leen, S. B., and O'Donoghue, P. E., "Cyclic Plasticity of Welded P91 Material for Simple and Complex Power Plant Connections," *Int. J. Fatigue*, Vol. 87, 2016, pp. 391–404, https://doi.org/10.1016/j.ijfatigue.2016.02.005

[35] Ding, X. and Zhang, G., "Coefficient of Equivalent Plastic Strain Based on the Associated Flow of the Drucker-Prager Criterion," *Int. J. Non Linear Mech.*, Vol. 93, 2017, pp. 15–20, https://doi.org/10.1016/j.ijnonlinmec.2017.04.018

[36] Stephenson, M., "Crack Prediction and Subsequent Simulation Driven Redesign of an Exhaust Manifold," presented at the *SIMULIA UK Regional User Meeting*, Cheshire, UK, Nov. 3–5, 2014, Dassault Systèmes, Johnston, RI, 10p.

[37] Liao, M., Okazaki, T., Ballarini, R., Schultz, A., and Galambos, T., "Nonlinear Finite-Element Analysis of Critical Gusset Plates in the I-35W Bridge in Minnesota," *J. Struct. Eng.*, Vol. 137, No. 1, 2011, pp. 59–68, https://doi.org/10.1061/(ASCE)ST.1943-541X.0000269

[38] Muránsky, O., Smith, M. C., Bendeich, P. J., Holden, T. M., Luzin, V., Martins, R. V., and Edwards, L., "Comprehensive Numerical Analysis of a Three-Pass Bead-in-Slot

Copyright by ASTM Int'l (all rights reserved); Wed Dec 4 09:43:32 EST 2019
Downloaded/printed by
Kansas University (Kansas University) pursuant to License Agreement. No further reproductions authorized.

Weld and Its Critical Validation Using Neutron and Synchrotron Diffraction Residual Stress Measurements," *Int. J. Solids Struct.*, Vol. 49, No. 9, 2012, pp. 1045–1062, https://doi.org/10.1016/j.ijsolstr.2011.07.006

[39] Džupon, M., Falat, L., Slota, J., and Hvizdoš, P., "Failure Analysis of Overhead Power Line Yoke Connector," *Eng. Fail. Anal.*, Vol. 33, 2013, pp. 66–74, https://doi.org/10.1016/j.engfailanal.2013.04.024

[40] Kaufmann, E., Metrovich, B., and Pense, A., "Characterization of Cyclic Inelastic Strain Behavior on Properties of A572 Gr. 50 and A913 Gr. 50 Rolled Sections," ATLSS Report No. 01-13, ATLSS, Lehigh University, Bethlehem, PA, 2001, 35p.

[41] Andrade, F. X. C., Feucht, M., Haufe, A., and Neukamm, F., "An Incremental Stress State Dependent Damage Model for Ductile Failure Prediction," *Int. J. Fract.*, Vol. 200, Nos. 1–2, 2016, pp. 127–150, https://doi.org/10.1007/s10704-016-0081-2

[42] Brocks, W. and Scheider, I., "Numerical Aspects of the Path-Dependence of the *J*-Integral in Incremental Plasticity," Technical Note GKSS/WMS/01/08, Institut für Werkstofforschung, GKSS Forschungszentrum, Geesthacht, Germany, 2011, 33p.

[43] Langill, T. J. and Schlafly, T., "Cope Cracking in Structural Steel after Galvanizing," *Mod. Steel Constr.*, Vol. 35, No. 10, 1995, pp. 40–45.

[44] Kuklik, V., "Post on the Issue of Safety of Steel Structures of Hot Dip Galvanized Structural Components," *Procedia Eng.*, Vol. 40, 2012, pp. 241–246, https://doi.org/10.1016/j.proeng.2012.07.087

[45] Elboujdaini, M., Tyson, W. R., and Goodwin, F., "Experiments on Delayed Failure during Galvanizing of Flame-Cut Structural Steels," presented at the *SIF 2004 Structural Integrity and Fracture*, Brisbane, Australia, Sept. 26–29, 2004, University of Queensland, Brisbane, Australia, 6p.

[46] ASTM A143/A143M-07, *Standard Practice for Safeguarding Against Embrittlement of Hot-Dip Galvanized Structural Steel Products and Procedure for Detecting Embrittlement*, ASTM International, West Conshohocken, PA, 2014, www.astm.org

[47] Minami, K., Mori, T., and Horikawa, H., "Stress Properties of Welded Portions by Hot Dip Galvanizing and Fatigue Test—Fatigue Strength of Welded Joins by Hot Dip Galvanizing (Report 1)," *Q. J. Jpn. Weld. Soc.*, Vol. 21, No. 4, 2003, pp. 576–583, https://doi.org/10.2207/qjjws.21.576

[48] Minami, K., Mori, T., and Horikawa, H., "Fatigue Test on Large-Scale Welded Girder Specimens with Hot Dip Galvanizing—Fatigue Strength of Welded Joints by Hot Dip Galvanizing (Report 2)," *Q. J. Jpn. Weld. Soc.*, Vol. 21, No. 4, 2003, pp. 584–591, https://doi.org/10.2207/qjjws.21.584

[49] Mori, T., Minami, K., and Horikawa, H., "Influence of Hot Dip Galvanizing Conditions and Steel on Fatigue Strength—Fatigue Strength of Welded Joints by Hot Dip Galvanizing (Report 3)," *Q. J. Jpn. Weld. Soc.*, Vol. 22, No. 2, 2004, pp. 272–281, https://doi.org/10.2207/qjjws.22.272

[50] Zerbst, U., Ainsworth, R. A., Beier, H. T., Pisarski, H., Zhang, Z. L., Nikbin, K., Nitschke-Pagel, T., Münstermann, S., Kucharczyk, P., and Klingbeil, D., "Review on Fracture and Crack Propagation in Weldments—A Fracture Mechanics Perspective," *Eng. Fract. Mech.*, Vol. 132, 2014, pp. 200–276, https://doi.org/10.1016/j.engfracmech.2014.05.012

[51] Kazakov, A., Kazakova, E., Karasev, M., Lubochko, D., and Lubochko, D., "Structural Investigation and Control of Multi-Pass Gas-Shielded Flux-Cored Arc Weldments," *Mater. Perform. Charact.*, Vol. 6, No. 3, 2017, pp. 256–270, https://doi.org/10.1520/MPC20160035

[52] James, M. N., "Designing against LMAC in Galvanised Steel Structures," *Eng. Fail. Anal.*, Vol. 16, No. 4, 2009, pp. 1051–1061, https://doi.org/10.1016/j.engfailanal.2008.05.019

[53] Nwachukwu, P. U. and Oluwole, O. O., "Effects of Rolling Process Parameters on the Mechanical Properties of Hot-Rolled St60Mn Steel," *Case Stud. Constr. Mater.*, Vol. 6, 2017, pp. 134–146, https://doi.org/10.1016/j.cscm.2017.01.006

[54] Kumar, V., "Improving Steel Processing Through Thermo-Mechanical Simulation Studies," *Mater. Perform. Charact.*, Vol. 4, No. 3, 2015, pp. 421–435, https://doi.org/10.1520/MPC20150008

Copyright by ASTM Int'l (all rights reserved); Wed Dec 4 09:43:32 EST 2019
Downloaded/printed by
Kansas University (Kansas University) pursuant to License Agreement. No further reproductions authorized.

[55] Pullaro, J. J., "Retrofit of Cracked Welded Steel Bridge Girders," *Extending the Life of Bridges, ASTM STP1100*, B. C. Brown, G. W. Maupin, and A. G. Lichtenstein, Eds., ASTM International, West Conshohocken, PA, 1990, pp. 18–31, http://dx.doi.org/10.1520/STP14538S

[56] Kaufmann, E. and Fisher, J. W., "The Effect of Straightening Method on the k Area Loading Behavior of Rolled Column Sections," ATLSS Report No. 01-16, ATLSS, Lehigh University, Bethlehem, PA, 2001, 31p.

Copyright by ASTM Int'l (all rights reserved); Wed Dec 4 09:43:32 EST 2019
Downloaded/printed by
Kansas University (Kansas University) pursuant to License Agreement. No further reproductions authorized.